Shape-Dependent Catalytic Properties of Pt Nanoparticles

Simon Mostafa,[†] Farzad Behafarid,[†] Jason R. Croy,[†] Luis K. Ono,[†] Long Li,[‡]
Judith C. Yang,[§] Anatoly I. Frenkel,[||] and Beatriz Roldan Cuenya*,[†]

*Department of Physics, University of Central Florida, Orlando, Florida 32816, United States,
Department of Mechanical Engineering and Materials Science, University of Pittsburgh,
Pittsburgh, Pennsylvania 15261, United States, Department of Chemical and Petroleum
Engineering, University of Pittsburgh, Pittsburgh, Pennsylvania 15261, United States, and
Department of Physics, Yeshiva University, New York, New York 10016, United States*

Received July 27, 2010; E-mail: roldan@physics.ucf.edu

Abstract: Tailoring the chemical reactivity of nanomaterials at the atomic level is one of the most important
challenges in catalysis research. In order to achieve this elusive goal, fundamental understanding of the
geometric and electronic structure of these complex systems at the atomic level must be obtained. This
article reports the influence of the nanoparticle shape on the reactivity of Pt nanocatalysts supported on
γ-Al$_2$O$_3$. Nanoparticles with analogous average size distributions ($\sim$0.8$-$1 nm), but with different shapes,
synthesized by inverse micelle encapsulation, were found to display distinct reactivities for the oxidation of
2-propanol. A correlation between the number of undercoordinated atoms at the nanoparticle surface and
the onset temperature for 2-propanol oxidation was observed, demonstrating that catalytic properties can
be controlled through shape-selective synthesis.

1. Introduction

Numerous studies have been devoted to understanding the
properties that affect the catalytic performance of metal nano-
particles (NPs) such as their size, interaction with the support,
and oxidation state.[1−5] The role played by the NP shape on
catalytic performance is, however, less understood. Furthermore,
the former parameters cannot be considered separately, since
the NP size as well as support will also impact the most stable
NP shapes, highlighting the complexity of real-world catalysts.
Previous reports have explained the distinct reactivity of NPs
with different shapes based on the presence of different
crystalline facets. For example, Xu et al.[6] demonstrated that
Ag nanocubes with predominantly {100} facets were signifi-
cantly more active for the oxidation of styrene than nanoplates
with mainly {111} planes, while nanospheres containing a
combination of both crystalline facets displayed intermediate
reaction rates.[6] Synergistic effects have also been reported, with
oxygen adsorption taking place on Pt{100} planes but its
reduction occurring at {111} facets after an intermediate step
of surface diffusion from the initial adsorption sites.[7] While these
studies have provided valuable insights, limitations with respect

to NP shape characterization at the subnanometer scale, where
NP catalysts display enhanced activities, have hindered the
detailed understanding of structure-dependent chemical reac-
tions. Recent advances in characterization methods[8,9] may
contribute to overcoming this hurdle. The present work addresses
shape-dependent changes in the reactivity of micellar Pt NPs
supported on nanocrystalline γ-Al$_2$O$_3$ using the oxidation of
2-propanol as a model reaction. The preparation method used
allows for a high degree of control over sample monodispersity
in terms of NP size as well as shape. Extended X-ray absorption
fine-structure spectroscopy (EXAFS) has been used in conjunc-
tion with high-angle annular dark-field scanning transmission
electron microscopy (HAADF-STEM) and modeling to obtain
the shapes of micellar Pt NPs in the $\sim$1 nm size range.[9] Samples
prepared under the same conditions, using the same support,
and possessing nearly identical size distributions were found
to display drastically different catalytic reactivities, correlating
with their geometry. In particular, decreasing onset reaction
temperatures for 2-propanol oxidation were observed with
increasing number of undercoordinated atoms at the NP's
surface.

2. Experimental Methods

a. Sample Preparation. Size- and shape-selected Pt NPs were
synthesized by encapsulating metal ions (H$_2$PtCl$_6$ precursor) inside
inverse micelles formed by dissolving polystyrene-*block*-poly(2-
vinylpyridine) (PS-P2VP) in toluene.[9,10] Two polymers with
different head lengths and various metal−salt/polymer−head ratios
were employed to create distinct NP geometries (see Table 1 and
ref 9 for details). Subsequently, the NP solution was impregnated
on nanocrystalline γ-Al$_2$O$_3$ supports ($\sim$40 nm average grain size,

† University of Central Florida.
‡ Department of Mechanical Engineering and Materials Science, Uni-
versity of Pittsburgh.
§ Department of Chemical and Petroleum Engineering, University of
Pittsburgh.
|| Yeshiva University.
(1) Haruta, A. *Chem. Rec.* **2003**, *3*, 75.
(2) Roldan Cuenya, B. *Thin Solid Films* **2010**, *518*, 3127.
(3) Freund, H.-J. *Top. Catal.* **2008**, *48*, 137.
(4) Cho, A. *Science* **2003**, *299*, 1684.
(5) Campbell, C. T. *Science* **2004**, *306*, 234.
(6) Xu, R.; Wang, D.; Zhang, J.; Li, Y. *Chem. Asian J.* **2006**, *1*, 888.
(7) Komanicky, V.; Iddir, H.; Chang, K. C.; Menzel, A.; Karapetrov, G.;
Hennessy, D.; Zapol, P.; You, H. *J. Am. Chem. Soc.* **2009**, *131*, 5732.

(8) Frenkel, A. I.; Hills, C. W.; Nuzzo, R. G. *J. Phys. Chem. B* **2001**,
105, 12689.

Table 1. Parameters Used for the Synthesis of Micellar Pt NPs Supported on γ-Al$_2$O$_3$: Diblock Copolymer, Metal−Salt to P2VP ratio (L), Annealing Temperature, and Percent of Oxygen in the Annealing Environment[a]

Sample	Polymer	L	annealing T (°C) [(% O$_2$)]	TEM diameter (nm)	EXAFS environment	path	N_1 (MS analysis)	N_1 (first shell)	R (Å)
S1	PS(27700)-P2VP(4300)	0.1	375 [50]	0.8 (2)	H$_2$	Pt−Pt	7.7 (4)		2.753 (5)
S2	PS(27700)-P2VP(4300)	0.2	375 [50]	1.0 (2)	H$_2$	Pt−Pt	9.1 (5)	8.7 (5)	2.765 (2)
					propanol + O$_2$	Pt−Pt	8.0 (4)	2.768 (2)	
						Pt−O		0.7 (2)	2.02 (2)
S3	PS(16000)-P2VP(3500)	0.05	375 [50]	1.0 (2)	H$_2$	Pt−Pt	7.5 (3)	7.1 (5)	2.745 (4)
					propanol + O$_2$	Pt−Pt	4.3 (1.3)	2.77 (1)	
						Pt−O		2.3 (5)	2.06 (2)
S4	PS(16000)-P2VP(3500)	0.1	425 [70]	1.0 (2)	H$_2$	Pt−Pt	8.7 (6)		2.746 (5)

[a] Information on the average NP diameter (STEM) and average first-nearest neighbor coordination number (N_1) obtained from multiple scattering (MS) analysis of EXAFS data are also shown. N_1 values, Pt−Pt, and Pt−O distances (R) extracted from the first-shell analysis of EXAFS spectra from S1−S4 acquired after H$_2$ reduction and from S2 and S3 after subsequent exposure to O$_2$ and 2-propanol at room temperature are also given. The N_1 values obtained for the reduced S2 and S3 samples from two different EXAFS analysis methods (MS and first-shell analysis) are within the error bars. Uncertainties in the last digit are given in parentheses.

Inframat Advanced Materials), and the polymer was removed by a 24-h annealing treatment in O$_2$ at 375 °C. No residual chlorine or carbon from the NP synthesis were detected in these samples after annealing via XPS (see Supporting Information Figure S1). The resulting samples contained 1−2% Pt by weight.

b. Sample Characterization. Information on the NP diameters was obtained from the analysis of HAADF-STEM images. EXAFS measurements were conducted at beamline X18B of the NSLS at Brookhaven National Laboratory after in situ NP reduction in H$_2$ at 375 °C and after subsequent simultaneous exposure to O$_2$ and 2-propanol. Details on the EXAFS characterization of these samples in H$_2$ at room and low temperature (from −85 to −108 °C) can be found in ref 9. The in situ experiments under reactant flow were carried out in an experimental setup analogous to that described in ref 11. Background subtraction from the EXAFS data obtained in the latter setup was done as follows. After the initial background subtraction by absolute minimization of the low r portion of the data, the data were further modified by minimizing the difference between the EXAFS theory and the experimental data.[12] This option is available in the IFEFFIT data analysis package used in this work.[13]

The catalytic properties of the reduced NPs for 2-propanol oxidation were measured in a continuous flow packed-bed reactor interfaced to a quadrupole mass spectrometer (QMS). Mass flow controllers were used to introduce the desired gases and alcohol vapor (bubbler configuration) into the system. The content of 2-propanol in the reactant stream was ~2%, with O$_2$ being ~20%. A similar O$_2$-rich oxidation environment was used for analogous reactivity tests by Centeno et al.[14] and Liu et al.[15] A total flow of 50 mL/min was maintained throughout the reactions using helium as carrier gas. The reactor itself consists of a quartz tube containing 50 mg of the powder sample supported by quartz wool plugs. The reactor is enclosed by a tubular furnace controlled via an external PID controller. The QMS monitors the composition of the gases leaving the reactor outlet. Conversion of 2-propanol under these conditions was measured in 10 °C increments in the range of 40−100 °C. The measurements were repeated at least twice on identical (same preparation batch) fresh samples.
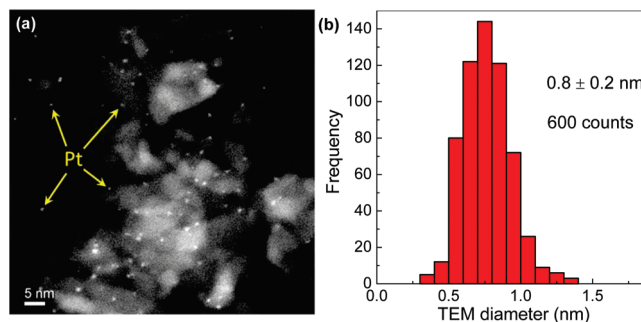
(9) Roldan Cuenya, B.; Croy, J. R.; Mostafa, S.; Behafarid, F.; Li, L.; Zhang, Z.; Yang, J. C.; Wang, Q.; Frenkel, A. I. *J. Am. Chem. Soc.* **2010**, *132*, 8747.
(10) Croy, J. R.; Mostafa, S.; Heinrich, H.; Roldan Cuenya, B. *Catal. Lett.* **2009**, *131*, 21.
(11) Estrella, M.; Barrio, L.; Zhou, G.; Wang, X.; Wang, Q.; Wen, W.; Hanson, J. C.; Frenkel, A. I.; Rodriguez, J. A. *J. Phys. Chem. C* **2009**, *113*, 14411.
(12) Newville, M.; Livins, P.; Yacoby, Y.; Rehr, J. J.; Stern, E. A. *Phys. Rev. B* **1993**, *47*, 14126.
(13) Ravel, B.; Newville, M. *J. Synchrotron Radiat.* **2005**, *12*, 537.
(14) Centeno, M. A.; Paulis, M.; Montes, M.; Odriozola, J. A. *Appl. Catal., A* **2002**, *234*, 65.
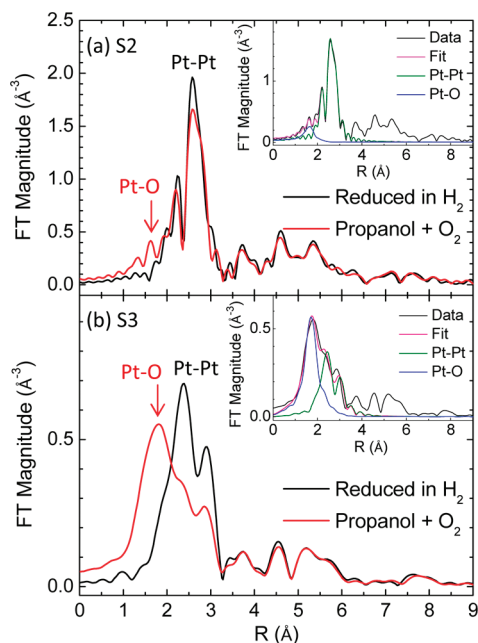(15) Liu, S. Y.; Yang, S. M. *Appl. Catal., A* **2008**, *334*, 92.

Figure 1. (a) HAADF STEM image of polymer-free micellar Pt NPs supported on γ-Al$_2$O$_3$ (S1). The image was taken after polymer removal and NP reduction in H$_2$ at 375 °C. (b) Histogram of the NP diameter obtained from STEM images.

3. Results

a. Morphological and Structural Characterization (STEM, EXAFS). Figure 1a shows a HAADF-STEM image of Pt NPs on γ-Al$_2$O$_3$ (S1) taken after polymer removal in O$_2$ at 375 °C and subsequent NP reduction in H$_2$ in the EXAFS cell. The corresponding histogram in Figure 1b provides clear evidence that the relatively narrow size distribution (diameter of 0.8 ± 0.2 nm, S1) resulting from our micellar NP synthesis is maintained throughout the deposition and annealing processes. In-depth STEM investigations of the remaining samples revealing the average NP diameters reported in Table 1 (1.0 ± 0.2 nm for S2, S3, and S4) are included in ref 9.

Figure 2 displays k^2-weighted EXAFS data from (a) S2 and (b) S3 acquired at room temperature after NP reduction in H$_2$ and subsequent exposure to O$_2$ and 2-propanol. The analysis of the spectra obtained under H$_2$ at room temperature only reveal metallic Pt signatures, while Pt−O species are detected at room temperature under reactant flow. The values of the coordination numbers for Pt−O and Pt−Pt species as well as the distances (first-shell EXAFS analysis) are included in Table 1. A decrease in the Pt−Pt coordination numbers is observed on the samples exposed to reactants along with the presence of Pt−O bonds. Additional information on the geometric structure of our NPs was extracted from EXAFS measurements taken in H$_2$ at room or low temperature (~ −85 to −108 °C).[9] The coordination numbers of the NPs in each sample were extracted up to the fourth nearest neighbor from a multiple scattering (MS) analysis of the EXAFS data. In combination with STEM (NP diameter), the coordination numbers define both the size and the shape of

Figure 2. k^2-weighted EXAFS data in r space obtained from (a) S2 and (b) S3 containing Pt NPs supported on γ-Al$_2$O$_3$. The spectra were acquired at room temperature after sample reduction in H$_2$ and after subsequent in situ exposure to O$_2$ and 2-propanol. The insets show the raw data measured under O$_2$ + 2-propanol flow together with the corresponding fits including two components: Pt–O and Pt–Pt. Fourier transform parameters are as follows: the k range is from (a) 2 to 18 Å^{-1} and (b) 3 to 11 Å^{-1}. The Hanning window sills are $\Delta k = 2$ Å^{-1}.

the NPs that can be obtained by modeling.[16] Table 1 compiles the first nearest-neighbor coordination numbers (N_1) extracted for all reduced Pt NP samples from MS analysis. A Pt atom in the bulk fcc structure has 12 bonds, while this number decreases for the atoms at the surface of NPs (atoms at steps, kinks and corners). The three shapes displaying the best agreement between model and experimental geometric parameters for each sample are displayed in Figure 3, where the color represents the number of first nearest neighbors ranging from 9 for atoms at {111} facets to 4 for corner atoms. The final model shapes included as the inset in Figure 5 were selected based on the minimization of the difference between experimental and model coordination numbers (N_1, N_2, and N_3) and NP diameters.

It should be noted that similar NP shape determination via EXAFS under these reaction conditions is extremely challenging and has not been implemented to date. The MS analysis required to extract reliable NP shape information must be conducted on high-quality EXAFS data, which are normally obtained only at low temperature, since a damping in the EXAFS signals, correlated with the increase in the dynamic disorder, is observed at elevated temperatures. Furthermore, no reliable structural model can be constructed to reproduce the shape of partially oxidized Pt NPs that might be present during an oxidation catalytic reaction; see Figure 2. The former is due in part to the similarity in the Pt–O distances reported for bulk Pt oxides with distinct structures ($\sim$1.99–2.04 Å for PtO and different structures of PtO$_2$).[17] Due to the above constraints, our NP shape determination has been limited to the metallic Pt NPs present in our samples before exposure to O$_2$ and 2-propanol. This shape

(16) Frenkel, A. I. *J. Synchrotron Radiat.* **1999**, *6*, 293.
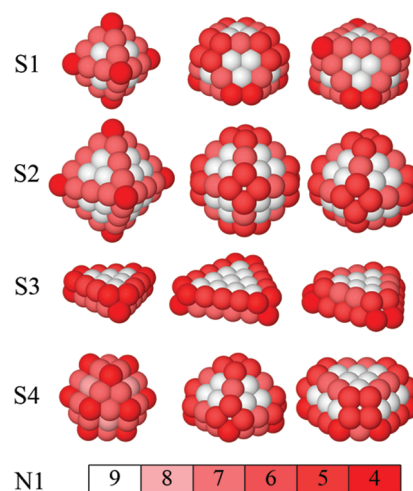(17) Seriani, N.; Jin, Z.; Pompe, W.; Ciacchi, L. C. *Phys Rev B* **2007**, *76*, 155421.

Figure 3. Three NP shapes that resulted in the best agreement with the coordination numbers obtained from the fits to the EXAFS data as well as with the TEM diameter measured for each of the Pt NP/γ-Al$_2$O$_3$ samples. The shapes that provided the best overall fit are shown in the left column. The color coding indicates the different number of first nearest neighbors (N_1) of surface atoms in each NP.
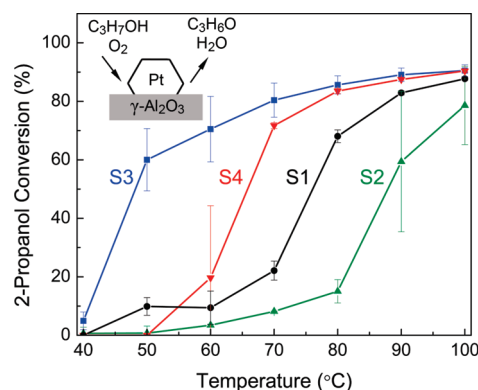

Figure 4. Conversion of 2-propanol during oxidation reactions. The catalyst samples containing micellar Pt NPs supported on nanocrystalline γ-Al$_2$O$_3$ have similar average diameters ($\sim$0.8 nm for S1 and $\sim$1 nm for S2, S3, and S4) but different shapes. The reactivity was measured in a packed-bed mass flow reactor by mass spectrometry. Error bars describe the maximum and minimum conversion observed at each given temperature under steady state conditions.

should be considered the starting point of a possibly dynamic NP structure under reaction conditions. Analysis (first shell only) of the EXAFS spectra of two samples (S2 and S3) measured in situ before and after reactant flow (Figure 2) has been implemented. Table 1 displays the N_1 values, Pt–Pt and Pt–O distances extracted from those fits. Interestingly, only a minor Pt–O signal was detected on the 3-dimensional particles from S2 (Figure 2a), while a significant content of oxidized Pt species was obtained for the 2D NPs in S3 (Figure 2b).

b. Catalytic Reactivity. Figure 4 shows temperature-dependent mass spectrometry data from the conversion of 2-propanol over Al$_2$O$_3$-supported Pt NPs during oxidation reactions. A short H$_2$ annealing at 375 °C prior to each experiment was carried out. For all samples, a clear onset reaction temperature is observed, as indicated by the abrupt increase of the activity, followed by a continued increase with temperature until reaching a maximum at $\sim$90 °C. The data displayed in Figure 4 correspond to steady state conditions at each temperature. Since the maximum conversion and selectivity observed in this temperature range is similar for all samples, the most critical
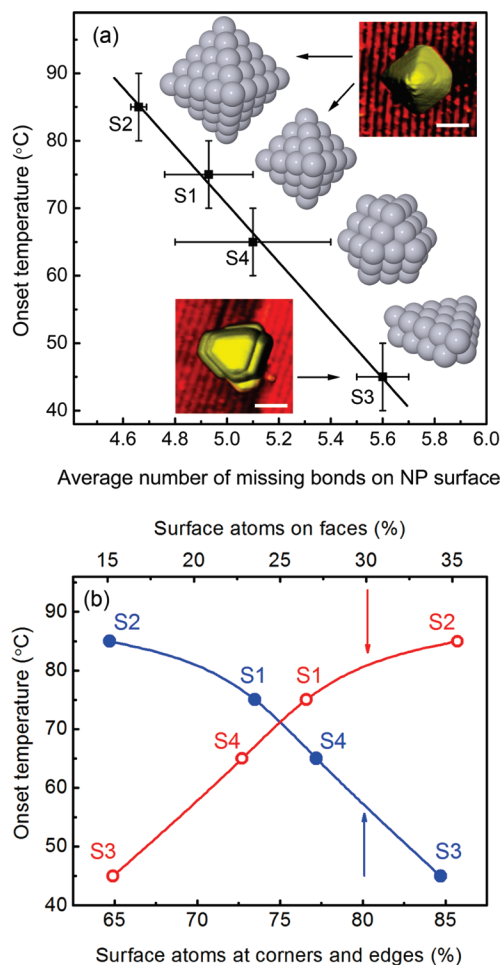
Figure 5. Onset temperature for 2-propanol oxidation over Pt NPs/γ-Al$_2$O$_3$ versus (a) the average number of missing bonds at the NP surface, N_m, and (b) the percentage of atoms at corners/edges and faces on the NP surface. The coordination numbers of the corner/edge atoms are 4−7, and those of the atoms at NP faces are 8−9. The solid lines are a guide for the eye. The insets in (a) display the model shapes that best describe the NPs in each of the samples (obtained from EXAFS and TEM measurements and modeling), together with STM images acquired on similarly synthesized but larger Pt NPs supported on TiO$_2$(110) after annealing in UHV at 1010 °C. The scale bars in the STM insets are 5 nm. The horizontal error bars in (a) indicate the range of N_m values obtained from the three shapes shown in Figure 2 for each sample. The vertical error bars in a describe the uncertainty in the determination of the onset reaction temperature.

parameter indicating catalyst performance under these conditions is the reaction onset temperature, considered hereafter as the temperature following the greatest increase (largest slope) in conversion. As such, S3 would be considered to have the best performance, as it displays the lowest onset temperature (∼50 °C). The inset in Figure 4 schematically indicates the predominant reaction pathway. No activity was observed for the Pt-free γ-Al$_2$O$_3$ support up to the maximum reaction temperature employed in this study of 100 °C. According to the literature, γ-Al$_2$O$_3$ becomes active only above ∼150 °C.[14,18]

To investigate the effect of particle shape on reactivity, the reaction onset temperature for each sample is compared with the average number of missing bonds of all atoms located at the NP surface (N_m) as estimated from the three NP shapes that best fit the experimental TEM diameters and EXAFS coordination numbers (Figure 3 and inset in Figure 5a). Supporting

Information Figure S2 also displays the conversion data obtained at 60 °C versus N_m, indicating increased overall 2-propanol conversion with increasing N_m. Figure 5a shows the reaction onset temperature for each of the catalyst samples studied as a function of N_m. For NPs of identical size (∼1 nm diameter for S2, S3, and S4), this figure shows a strong correlation between catalytic activity and NP shape, demonstrating that an increase in N_m is accompanied by a decrease in the onset reaction temperature, with the 2D NPs in S3 displaying the best catalytic performance. Scanning tunneling microscopy (STM) images of larger but similarly synthesized Pt NPs supported on TiO$_2$(110) are also shown as insets in Figure 5a. It should be noted that the STM images were acquired on NP samples subjected to a different pretreatment (annealing in UHV at 1010 °C), which could play a role on the final NP shape obtained. Nevertheless, our STM images indicate that the model shapes extracted from the synergistic combination of EXAFS and STEM are a reasonable representation of typical real cluster shapes obtained from inverse micelle synthesis methods. Figure 5b displays the correlation between reaction onset temperature and the percentage of surface atoms at corners/edges and faces.

Under our experimental conditions, a conversion greater than 80% was achieved for all Pt NP/γ-Al$_2$O$_3$ samples, and the formation of acetone, CO$_2$, and water was observed. Such products are expected to derive from partial and complete oxidation of 2-propanol, as shown below:

$$C_3H_7OH + 1/2\ O_2 \rightarrow C_3H_6O + H_2O \qquad (1)$$

$$C_3H_7OH + 9/2\ O_2 \rightarrow 3CO_2 + 4H_2O \qquad (2)$$

The partial oxidation (pathway 1) was the dominant reaction for all samples below 100 °C, with over 90% selectivity. No signs of catalyst poisoning were observed within the temperature range studied, and no change in the selectivity was detected in the course of the reaction up to the maximum reaction temperature of 100 °C. More specifically, if the Pt NPs would have deactivated, conversion rates would be expected to decrease and reactions taking place mainly over the γ-Al$_2$O$_3$ support, i.e., 2-propanol dehydration to propene and water, would become dominant.[19,20] However, reaction rates consistently increased with increasing temperature, and formation of propene was never observed under our reaction conditions. The total oxidation of 2-propanol was found to occur for these NPs, under analogous experimental conditions, in the 100−200 °C temperature range, which is consistent with earlier reports.[20]

4. Discussion

The samples studied here were all prepared using inverse micelle encapsulation methods and subject to analogous pretreatment conditions. Furthermore, their characterization in terms of composition (XPS, Supporting Information Figure S1) and particle diameter (STEM) showed virtually no differences among them (with the exception of S1 having a slightly smaller diameter). However, our reactivity experiments reveal distinct catalytic properties for the different samples. The EXAFS results demonstrate a similar phenomenon, where seemingly same-sized particles (e.g., S3 and S4) display clear differences in the coordination numbers (N_1 in Table 1) and in bond-length

(18) Kulkarni, D.; Wachs, S. E. *Appl. Catal., A* **2002**, *237*, 121.

(19) Zhang, J. H.; Zhou, X. L.; Wang, J. A. *J. Mol. Catal. A* **2006**, *247*, 222.

(20) Burgos, N.; Paulis, M.; Antxustegi, M. M.; Montes, M. *Appl. Catal., B* **2002**, *38*, 251.

disorder.[9] In particular, the reduced N_1 value obtained for S3 as compared to S4, both measured on reduced samples under H_2 atmosphere, can only be understood if flatter NPs (2D shape) that have a larger number of undercoordinated atoms (e.g., those at the NP surface and perimeter) are present in S3. While N_1 for bulk Pt is 12, our NPs show significantly lower values (e.g., $N_1 = 7.5 \pm 0.3$ for S3) due to surface truncation effects. Furthermore, when comparing two polyhedral NPs, the largest N_1 value will be observed for the most symmetric (quasi-spherical) NP shape.

The different polymers and metal−salt/polymer−head molecular ratios used during the NP synthesis (see Table 1) were found to have an impact upon the final size and shape of the NPs formed. The size of the NPs can be tuned by changing the molecular weight of the polymer core (P2VP) as well as by changing the metal−salt to polymer core ratio (L, in Table 1). The latter effect explains the smaller size of the NPs in S1 as compared to S2. In addition, the spherical micelles formed by dissolving PS-P2VP diblock-copolymers in toluene generally lead to 3D cluster shapes upon metal loading. Nevertheless, for NPs in the 1 nm size range, our EXAFS data indicate that their final shape is also influenced by the strength of NP/support interactions. For strongly interacting systems, such as Pt/γ-Al_2O_3,[21,22] 2D NP shapes can be obtained after annealing when low metal loadings and polymers with small core sizes (P2VP) are employed in the synthesis (S3).

The above results suggest that the differences in the catalytic performance observed for samples with similar average TEM diameter but different shape (Figures 4 and 5) are due to geometric effects, with undercoordinated Pt atoms at the NP surface constituting the most active reaction sites.[23−26] Interestingly, in Figure 5a the lowest onset temperature for 2-propanol oxidation is observed for the 2D bilayer NPs (S3). It should be noted that bilayer metal films have previously been shown to exhibit enhanced reactivity by Chen and Goodman.[27] In addition, flatter NP geometries result not only in an increased number of atoms at the surface but also in a greater contact area with the support and a larger number of perimeter atoms. A larger number of atoms in contact with the NP support might be beneficial for the catalytic reaction since the support itself could be involved, for example, by means of charge transfer to the NPs, strain-induced changes in the electronic properties of the supported NPs, or providing additional active sites for the adsorption of reactants.[1,28−36]

The correlation extracted from Figure 5a is useful in understanding the role of different atomic sites in the reactivity of supported nanocatalysts. The decreasing onset temperature for 2-propanol oxidation observed with increasing number of missing bonds (relative to bulk coordination) indicates that undercoordinated Pt atoms are the most active sites for this reaction. While Figure 5a shows the average number of missing bonds, it should be noted that corner atoms have a greater number of missing bonds (lower coordination) than atoms at steps, and the latter would have more missing bonds than a crystalline plane (see the color coding in Figure 3). Therefore, the results in Figure 5a suggest that atoms at specific surface sites on the NP play a dominant role in the catalytic process. This can be seen in Figure 5b, where the reaction onset temperature is displayed as a function of the percentage of atoms at corners and edges (coordination 4−7) on the NP surface. The lowest onset temperature is observed for the sample with the highest percentage of corner and edge atoms (S3).

While the methods used in this study cannot provide detailed information on the reaction mechanism, the enhanced catalytic performance observed for the 2D NPs with the largest number of perimeter atoms (S3) suggests that the γ-Al_2O_3 support might be involved. According to the literature, 2-propanol is likely adsorbed over the γ-Al_2O_3 surface due to this substrate's acidic nature[37−39] and subsequently interacts with oxygen atoms chemisorbed on the Pt clusters following dissociative adsorption.[40] This leads to the formation of acetone and water via oxidative dehydrogenation of 2-propanol. The latter mechanistic view supports the hypothesis that Pt oxide species may play an active role in alcohol oxidation reactions.[10,18,41−47] This is also confirmed by preliminary in situ EXAFS experiments (Figure 2), which indicate that the active Pt NP catalysts remain oxidized during this reaction. Furthermore, the higher content of Pt−O species detected on S3 after exposure to the reactants at room temperature suggests its more facile oxidation (more favorable dissociation of O_2). If Pt−O species on the NP surface are involved in this catalytic reaction through a Mars−van Krevelen-like process, the latter finding might explain the superior catalytic performance of S3 as compared to, for example, S2. Following this hypothesis, the oxidized surface of our NPs could

(21) Sanchez, S. I.; Menard, L. D.; Bram, A.; Kang, J. H.; Small, M. W.; Nuzzo, R. G.; Frenkel, A. I. *J. Am. Chem. Soc.* **2009**, *131*, 7040.

(22) Kwak, J. H.; Hu, J.; Mei, D.; Yi, C.-W.; Kim, D. H.; Peden, C. H. F.; Allard, L. F.; Szanyi, J. *Science* **2009**, *325*, 1670.

(23) Mavrikakis, M.; Stoltze, P.; Norskov, J. K. *Catal. Lett.* **2000**, *64*, 101.

(24) Lopez, N.; Janssens, T. V. W.; Clausen, B. S.; Xu, Y.; Mavrikakis, M.; Bligaard, T.; Norskov, J. K. *J. Catal.* **2004**, *223*, 232.

(25) Norskov, J. K.; Bligaard, T.; Hvolbaek, B.; Abild-Pedersen, F.; Chorkendorff, I.; Christensen, C. H. *Chem. Soc. Rev.* **2008**, *37*, 2163.

(26) Wu, X.; Senapati, L.; Nayak, S. K.; Selloni, A.; Hajaligol, M. *J. Chem. Phys.* **2002**, *117*, 4010.

(27) Chen, M. S.; Goodman, D. W. *Science* **2004**, *306*, 252.

(28) Grunwaldt, J. D.; Baiker, A. *J. Phys. Chem. B* **1999**, *103*, 1002.

(29) Meyer, R.; Lemire, C.; Shaikhutdinov, S. K.; Freund, H. *Gold Bull.* **2004**, *37*, 72.

(30) Rodriguez, J. A.; Vines, F.; Illas, F.; Liu, P.; Takahashi, Y.; Nakamura, K. *J. Chem. Phys.* **2007**, *127*, 211102.

(31) Sanchez, A.; Abbet, S.; Heiz, U.; Schneider, W. D.; Hakkinen, H.; Barnett, R. N.; Landman, U. *J. Phys. Chem. A* **1999**, *103*, 9573.

(32) Matthey, D.; Wang, J. G.; Wendt, S.; Matthiesen, J.; Schaub, R.; Laegsgaard, E.; Hammer, B.; Besenbacher, F. *Science* **2007**, *315*, 1692.

(33) Lima, F. H. B.; Zhang, J.; Shao, M. H.; Sasaki, K.; Vukmirovic, M. B.; Ticianelli, E. A.; Adzic, R. R. *J. Phys. Chem. C* **2007**, *111*, 404.

(34) Greeley, J.; Norskov, J. K.; Mavrikakis, M. *Annu. Rev. Phys. Chem.* **2002**, *53*, 319.

(35) Chen, J. G.; Menning, C. A.; Zellner, M. B. *Surf. Sci. Rep.* **2008**, *63*, 201.

(36) Lonergan, W. W.; Xing, X.; Zheng, R.; Qi, S.; Huang, B.; Chen, J. G. *Catal. Today* **2010**, in press; doi:10.1016/j.cattod.2010.05.014.

(37) Padilla, J. M.; Del Angel, G.; Navarrete, J. *Catal. Today* **2008**, *133*, 541.

(38) Ishikawa, A.; Komai, S.; Satsuma, A.; Hattori, T.; Murakami, Y. *Appl. Catal., A* **1994**, *110*, 61.

(39) Hua, W. M.; Gao, Z. *Appl. Catal., B* **1998**, *17*, 37.

(40) Augustine, R. L.; Doyle, L. K. *J. Catal.* **1993**, *141*, 58.

(41) Fu, Q.; Saltsburg, H.; Flytzani-Stephanopoulos, M. *Science* **2003**, *301*, 935.

(42) Hendriksen, B. L. M.; Frenken, J. W. M. *Phys. Rev. Lett.* **2002**, *89*, 046101.

(43) Shumbera, R. B.; Kan, H. H.; Weaver, J. F. *J. Phys. Chem. C* **2008**, *112*, 4232.

(44) Wang, J. G.; Li, W. X.; Borg, M.; Gustafson, J.; Mikkelsen, A.; Pedersen, T. M.; Lundgren, E.; Weissenrieder, J.; Klikovits, J.; Schmid, M.; Hammer, B.; Andersen, J. N. *Phys. Rev. Lett.* **2005**, *95*, 256102.

(45) Hegde, M. S.; Madras, G.; Patil, K. C. *Acc. Chem. Res.* **2009**, *42*, 704.

(46) Ackermann, M. D.; Pedersen, T. M.; Hendriksen, B. L. M.; Robach, O.; Bobaru, S. C.; Popa, I.; Quiros, C.; Kim, H.; Hammer, B.; Ferrer, S.; Frenken, J. W. M. *Phys. Rev. Lett.* **2005**, *95*, 255505.

(47) Yates, R. C.; Turner, J. E.; Gellman, A. J.; Somorjai, G. A. *Surf. Sci.* **1985**, *149*, 175.

provide the oxygen needed for the oxidation of 2-propanol, being subsequently replenished by the dissociation of molecular oxygen from the reactant flow. Since the energy barrier for oxygen dissociation at low coordinated sites (corner and edges) is expected to be lower, the higher number of such sites in S3 as compared to the rest of the samples would explain the higher increase in catalytic performance observed for this sample at the lowest temperature. Future in situ EXAFS experiments will be directed to further clarify the mechanistic details of the shape-dependent catalytic reactivity described here.

5. Conclusions

We demonstrated that micelle encapsulation methods are ideal synthesis routes for producing model systems for catalysis studies composed of size- and shape-selected NPs. Such a degree of monodispersity is critical in improving our understanding of the properties that control the performance of nanocatalysts. Our work shows that Pt NPs of similar size ($\sim$0.8$-$1 nm diameter) but different geometric structure (shape) display distinct catalytic properties. In particular, a decreasing onset reaction temperature for 2-propanol oxidation was observed with increasing number of missing bonds at the NP surface. Our findings highlight the idea that undercoordinated Pt surface atoms (corner and edge atoms) are the most active reaction sites. Acetone and water were generated as the main products below 100 °C, indicating that partial oxidation is the dominant reaction for this temper-

ature range. Our study demonstrates the value of a synergistic approach taking advantage of a variety of experimental methods to gain insight into the structure and reactivity of complex nanoscale systems relevant to the field of heterogeneous catalysis.

Supporting Information Available: XPS data from the C-1s and Cl-2p core level regions of Pt NPs supported on γ-Al$_2$O$_3$ taken before and after polymer removal, and information on the change in the conversion of 2-propanol at 60 °C as a function of the number of missing bonds on the NP surface. This material is available free of charge via the Internet at http://pubs.acs.org.

JA106679Z